PCCP

Accepted Manuscript

This article can be cited before page numbers have been issued, to do this please use: J. M. López Martí, N. J. English and M. G. Del Popolo, *Phys. Chem. Chem. Phys.*, 2018, DOI: 10.1039/C8CP00958A.

This is an Accepted Manuscript, which has been through the Royal Society of Chemistry peer review process and has been accepted for publication.

Accepted Manuscripts are published online shortly after acceptance, before technical editing, formatting and proof reading. Using this free service, authors can make their results available to the community, in citable form, before we publish the edited article. We will replace this Accepted Manuscript with the edited and formatted Advance Article as soon as it is available.

You can find more information about Accepted Manuscripts in the author guidelines.

Please note that technical editing may introduce minor changes to the text and/or graphics, which may alter content. The journal's standard Terms & Conditions and the ethical guidelines, outlined in our author and reviewer resource centre, still apply. In no event shall the Royal Society of Chemistry be held responsible for any errors or omissions in this Accepted Manuscript or any consequences arising from the use of any information it contains.

ROYAL SOCIETY OF CHEMISTRY

rsc.li/pccp

View Article Online
DOI: 10.1039/C8CP00958A

Elucidating Mysteries of Phase-Segregated Membranes: Mobile-Lipid Recruitment Facilitates Pores' Passage to the Fluid Phase

Jesús M. López Martí,[1] Niall J. English[2] and Mario G. Del Pópolo[1,3] *

[1]*CONICET & Facultad de Ciencias Exactas y Naturales, Universidad Nacional de Cuyo, Padre Jorge Contreras 1300, CP5500, Mendoza, Argentina.*

[2]*School of Chemical and Bioprocess Engineering, University College Dublin, Belfield, Dublin 4, Ireland.*

[3]*Atomistic Simulation Centre, School of Mathematics and Physics, Queen's University Belfast, University Road, Belfast BT7 1NN, UK.*

Phase segregation of multicomponent lipid bilayers leads to, under phase-coexistence conditions, domain formation, featuring delimitation by essentially one-dimensional borders. (Micro-)phase segregation of bilayers is proposed to influence the physiological behaviour of cell membranes and provides the driving force for lipid-raft formation. Experiments show a maximum on the electrical-conductivity of membranes at the phase-transition point, which has been conjectured to arise from border-nucleated transmembrane-conducting defects or pores. However, recent electroporation experiments on phase-segregated bilayers demonstrate electro-pore detection in the liquid disordered phase (L_d), wherein they diffuse over macroscopic periods without absorption into the liquid ordered phase (L_o). Here, we scrutinise transmembrane-pore formation via molecular dynamics simulations on a multicomponent phase-segregated bilayer. We find that pores created in L_o domains always migrate spontaneously to the L_d phase, via 'recruitment' of unsaturated lipids to the pore's rim to transport the pore to the fluid phase under a large stress-field driving force. Once in L_d domains, pores migrate towards their centre, never returning or pinning to L_o. These findings are explained by thermodynamics. By comparing the free-energy cost for creating pores in the bulk of L_d and L_o membranes, and in the phase-segregated system, we show that it is always more energetically tractable to create pores in L_d domains, independently of the pore size.

* Corresponding author: mdelpopolo@fcen.uncu.edu.ar & m.delpopolo@qub.ac.uk

View Article Online
DOI: 10.1039/C8CP00958A

Multicomponent lipid bilayers demix or phase-segregate at a temperature dependent on the membrane's chemical composition; under phase-coexistence conditions, this leads to the formation of domains that are delimited by domain borders. Lipid bilayers are two-dimensional structures, so domain borders are, *ipso facto*, one-dimensional soft wavering interfaces.[1,2] Indeed, phase and micro-phase segregation of bilayers have been proposed to influence the physiological behaviour of cell membranes, and provide the driving force for the formation of lipid rafts.[1-4] Typically, the two co-existing lipid phases have differing mechanical properties: one, termed the Liquid-Disordered phase (L_d), remains fluid, whilst the other (raft-like), denoted the Liquid-Ordered phase (L_o), evinces more solid-like behaviour. One intriguing aspect of lipid bilayers is that, even in the absence of ion-conducting protein channels, their electrical conductivity displays quantized current events and a sharp maximum at the phase-transition point.[1,5-7] Moreover, such enhanced ionic permeability coincides with the increasing heat capacity and lateral compressibility (i.e., enhanced area fluctuations) that occur near the phase transition point. One possible interpretation to rationalise these observations is that domain borders provide nucleation centres for the formation of transmembrane ion-conducting defects or pores.[1,7] However, recent electroporation and optical single-channel recording experiments on phase-segregated bilayers demonstrate electro-pore detection in the L_d phase, wherein they diffuse over macroscopic periods without absorption or pinning to L_o domains.[8] Although these advanced experiments still sense membranes over microscopic time- and length-scales, they seem to challenge the hypothesis that domain borders nucleate transmembrane pores.

The mechanisms and thermodynamics of pore nucleation in bio-membranes have been investigated with different theoretical methods, ranging from intuitive phenomenological models, such as Classical Nucleation Theory,[9] to elaborate formulations of Density Functional and Mean-Field theories.[20] As well documented in ref. 11, computer simulations have played an important role in shaping our understanding of the structural details and dynamical aspects of membrane poration[12-16] and electroporation.[17-19] For instance, both atomistic and coarse-grained simulations have revealed that the nucleation of a pore in a fluid lipid-phase occurs in two stages:[9,12-15] in the first, a small, irregular and hydrophobic defect is formed, which 'seeds' subsequently the growth of a larger hydrophilic trans-membrane pore. Further details on the complexities of membrane defects, as well as their key underlying role given the membrane phase state, are discussed with acuity in references 9,20-22.

View Article Online
DOI: 10.1039/C8CP00958A

Phase segregation in lipid bilayers has also been investigated using a variety of computational models and techniques.[1-4] Of particular relevance in the present context is the seminal work of Risselada *et al*., who investigated demixing and rafts formation in a three-components membrane by means of Molecular-Dynamics (MD) simulations based on the MARTINI coarse-grained model.[3] It was observed that spontaneous separation of a saturated phosphatidylcholine (PC)/ unsaturated PC/cholesterol mixture into L_d and L_o domains took place on times scale of several microseconds, at temperatures below the experimental mixing temperature. The structural and dynamical properties of the resulting phases were in good accord with experiments, and the simulations predicted a small line tension between domains (3.5 pN) and a short-ranged effective repulsion between domain borders.[3]

Motivated by the apparent contradiction between the standard interpretation of the membrane's conductance maximum near a phase transition, and the direct observation of electro-pores in liquid-disordered domains, we investigate in the present study transmembrane-pore formation on a phase-segregated lipid bilayer. As in ref. 3, our membrane is formed by the lipids dipalmitoyl-phosphatidylcholine (DPPC), dilinoleyl-phosphatidylcholine (DIPC), and cholesterol. We resort to coarse-grained Molecular-Dynamics simulations. From a mechanistic perspective, we show that pores of varying sizes created in L_o domains always migrate, spontaneously, to the L_d phase by 'recruitment' of mobile (unsaturated) lipids to the pore's rim, which carry the pore to the fluid L_d phase under the driving force of a large stress field, never to return to L_o. This central finding is readily explained by thermodynamics. By comparing the free-energy cost for creating pores of different sizes in the bulk of L_d and L_o membranes, and in the phase-segregated system, we show that it is always more energetically tractable to create pores in L_d domains, independently of the pore size. On one side, our results explain why electro-pores are experimentally observed in L_d; on the other, they put a quantitative note on the effect of domain borders on transmembrane pore nucleation. Although previous simulations have shown that phase-segregated membranes (electro-)porate more easily in L_d domains,[19] we discuss here the thermodynamic basis of pore formation in demixed bilayers, as well as a line-tension moderation mechanism that operates the transport of membrane pores under such conditions.

As a starting point, we have used the MARTINI forcefield[11] under the conditions of ref. 3. The choice of system is motivated by the fact that the composition of the two phases

View Article Online
DOI: 10.1039/C8CP00958A

predicted by MARTINI agrees well with the compositional analysis of phase-separated DIPC/DPPC/cholesterol vesicles measured by NMR. Initially a lipid bilayer was prepared by random distribution of DIPC (452), DPPC (452) and cholesterol (488). The membrane was solvated with 18,071 non-polarizable coarse-grained water beads. The system was equilibrated for 2 μs, allowing for the formation of two segregated domains, with a further 2 μs production run. Local membrane composition (DPPC:DIPC:CHOL) and curvature fluctuations were evaluated and collected during the production run. All simulations were run with GROMACS-4.6.5,[23,24] under anisotropic NPT conditions with $P_{xx} = P_{yy} = P_{zz} = 1$ bar and T = 295K. Electrostatic interactions were computed using the Particle-Mesh Ewald approach;[25-26] Lennard-Jones potentials were cut off at 1.2 nm. The final average dimensions of the membrane patch were $L_x = 25.5$ and $L_y = 12.78$ nm. Figure S1 (cf. Supplementary Information, ESI) shows each component's mole fraction along the direction perpendicular to the domain borders (*i.e.*, along the laboratory *x*-axis). In agreement with ref. 3, the resulting L_o domain is rich in DPPC and has a bulk composition of (0.67:0.04:0.29). The L_d domain, reach in DIPC, has a composition of (0.07:0.81:0.12).

Transmembrane-pore nucleation was investigated by standard umbrella sampling (US), applying harmonic restraining potentials of the form $V_o(\xi) = \frac{1}{2} K_o (\xi - \xi_o)^2$, where K_o is the force constant and ξ_o is the order parameter's reference position in the o^{th} US-window. ξ is the collective reaction coordinate developed properly discussed by Tolpekina et al.,[12,14-16] $\xi = (\Sigma - \Sigma_0) / (\Sigma_M - \Sigma_0)$, where $\Sigma = \sum_{i=1}^{N_l} \tanh(s|\boldsymbol{r}_i - \boldsymbol{r}_p|)$. In this equation, the summation is over all membrane atoms, N_l, and $|\boldsymbol{r}_i - \boldsymbol{r}_p|$ denotes the lateral distance, measured parallel to the bilayer plane, between the i^{th} lipid atom and the pore centre $\boldsymbol{r}_p$. The position of the pore centre is found self-consistently as detailed in ref 15. Consequently, the pore moves to find its energetically-preferred location within the membrane. *s* is a scaling factor, set to 1 nm^{-1} in all cases, that controls the maximum size of the pore for a given membrane patch. Σ_M is the largest possible system Σ value, *i.e.* $\Sigma_M = N_l$, whilst Σ_0 is the average equilibrium Σ value obtained from an unrestrained 2 μs simulation of a non-perforated membrane. The reaction coordinate ξ takes values between nearly zero for an unrestrained membrane, and unity when the membrane bears the largest pore. Notice that the size of the largest pore ($\xi \rightarrow 1$) is controlled by the value of *s*. Setting *s* to 1 nm^{-1} leads to pore radii of 1.5-2.5nm, depending on the membrane composition, when ξ approaches 1. Slightly negative ξ values occur when the lipid density at the pore centre exceeds the membrane's average equilibrium value during

View Article Online
DOI: 10.1039/C8CP00958A

natural fluctuations. With the above definition of the reaction coordinate, restraining ξ to a positive value is equivalent to decreasing the lipid density around $\boldsymbol{r}_p$. Moreover, scanning increasing ξ leads to pores of increasing size.

The calculation of ξ was implemented in PLUMED-2.0.2.[27,30] More than 40 US windows spanning ξ values between -0.1 and 1, were generated by shifting the restraint reference point, ξ_0, and run separately for 100 ns under anisotropic NPT conditions at 295K. Free-energy profiles, $\Delta G(\xi)$, were recovered from the ξ-time series via Weighted Histogram Analysis (WHAM)[28] and subsequently transformed to a pore radius representation, $\Delta G(R)$, by appropriate reweighting. To map ξ to a pore radius $R(\xi)$, we employed a Monte Carlo (MC) algorithm as described in references 12 and 15. For a given membrane configuration, $M=10^7$ uniformly-sampled random positions were generated on the X-Y plane of the simulation cell. Whenever the distance, r_{xy}, between a random point and the X-Y position of a phospholipid atom was smaller than a cut-off σ, the trial position was considered to be inside the van der Waals sphere of the atom and was discarded. Consequently, accepted random trials concentrated within the perimeter pore's projection on the X-Y plane. The effective pore radius was then computed as $R=\sqrt{(A_{\mathrm{box}}/\pi)}\times(M_c/M)$, where A_{box} is the area of the simulation box and M_c is the accepted-trial count. This procedure was executed for every configuration that contributed to the p(ξ) histogram of each US window. A σ-value of 0.3 nm lead to $R\sim0$ in a non-perforated membrane. Final $R(\xi)$ mappings are shown in Fig. S5 of ESI.

After the 4 μs simulation, pores of three different sizes (ξ_0 = 0.5, 0.6, 0.8, corresponding to R~0.3, 0.5 and 1.0 nm) were created at the centre of the L_o domain (cf. Fig. 1). For each pore, two independent 2 μs harmonic-restrained trajectories captured ξ fluctuations around the pre-specified ξ_0 - preventing spontaneous pore collapse. In all cases, the pore, sitting at the region of maximal membrane curvature, induces immediately local membrane bending. Concomitantly, the pore rim, which contained initially mostly DPPC and cholesterol (Fig. 2 – middle panel), commences recruiting unsaturated (mobile) lipids (cf. Fig. 1, second panel), so the pore migrates toward the fluid phase, eventually crossing one of the domain borders, staying at the L_d-slab centre. For ξ_0 = 0.6 and 0.8, the pores are hydrophilic; water clearly crosses the bilayer. This is highlighted in green in Fig. 1. For ξ_0 = 0.5, the pore is hydrophobic. In all cases, once the pore reaches L_d, the bending stress is released and the membrane flattens (cf. Fig. 1, right).

View Article Online
DOI: 10.1039/C8CP00958A

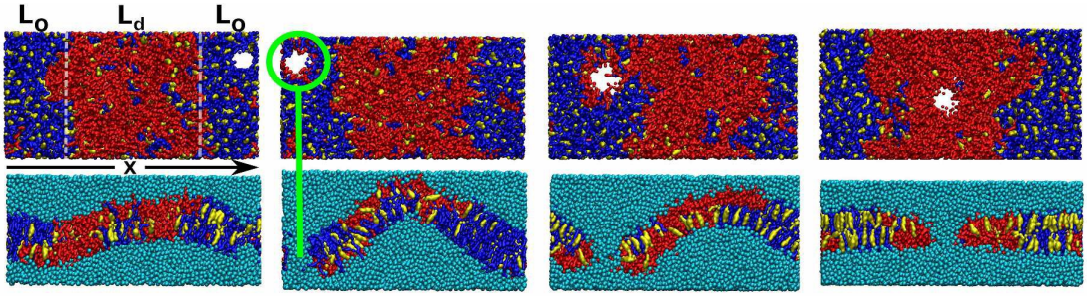

Figure 1: *Time evolution of a transmembrane pore in a phase segregated DPPC(Blue):DIPC(Red):CHOL(Yellow) bilayer. The order parameter ξ is harmonically restrained to ξ_0=0.8 (R~1nm). The time progression of the sequence is, from left to right, 0.01→ 0.073 → 0.25 → 1.7*μs*. The pore, created at the centre of the L_o domain, is hydrophilic; water clearly crosses the bilayer - highlighted in green. In all cases investigated (ξ_0 = 0.5, 0.6, 0.8), the pore, sitting at the region of maximal membrane curvature, induces immediately local membrane bending. Concomitantly, the pore rim, which contained initially only DPPC and cholesterol commences recruiting unsaturated (mobile) DIPC lipids (second panel), so the pore migrates toward the fluid phase, eventually crossing one of the domain borders, staying at the L_d-slab centre. Once the pore reaches L_d, bending stress is released and the membrane flattens (right panels). Movie files provided as Supplementary Material.*

In Fig. 2 we depict, for the largest pore (ξ_0 = 0.8), the time evolution of the closest pore-to-domain distance (*d*), the border composition ($X_{i,\,\mathrm{border}} = N_i / (N_{\mathrm{DPPC}} + N_{\mathrm{DIPC}} + N_{\mathrm{Chol}})$) and the pore radius (*R*). The identification of the domain borders was done as in ref. 3. The phosphate beads of DPPC were projected on a 2D grid spanning the X-Y plane of the simulation cell; grid points falling within a distance of 0.4 nm of the projected beads were marked as L_o domain elements. A cluster detection algorithm was then used to identify the L_o domain as the largest connected cluster of L_o elements, and the corresponding domain border. Negative *d*-values in Fig 2 mean that the pore centre is in L_o. The *d*-curve shows that the pore crosses the border within a fraction of microsecond and becomes confined at the L_d-domain centre. The arrow-marked point corresponds to the configuration shown in the final panel of Fig. 1. The $X_{i,\,\mathrm{border}}$ plot demonstrates that the pore rim is initially rich in DPPC and cholesterol, but with DIPC recruitment, still within the L_o domain (d<0), the border composition changes while the pore migrates and plateaus after ~1 μs upon pore stabilisation. As evidenced by the time evolution of the pore radius (bottom panel of Fig.2, and Fig. S2 ESI), large-pore sizes are relatively invariant whilst crossing domains. The opposite happens for smaller pores,

View Article Online
DOI: 10.1039/C8CP00958A

which shrink when crossing. In general, pores of equal size show very similar R-t traces (Fig. S2 ESI) and cross the domain border more or less at the same time. This is no coincidence, however. Before reaching the centre of the L_d domain the motion of the pore is not entirely random, as there is a large mechanical driving force that pushes the pore away from the more rigid phase. Considering that at the start of the simulations each pore was placed at the same distance from the domain border, *i.e.* at the centre of the L_o domain, pores of similar size end up reaching the domain border within similar time frames.

The simulations show that whenever the pore is within L_o, membrane bending and composition mismatch between the upper and lower leaflets depend little on pore size. Such mismatch is evident from the first three bottom panels of Fig. 1. To quantify these effects, we computed the bilayer's excess area and the mismatch area between domains (cf. ESI). The excess area is the difference between the actual surface area of the undulated membrane and the simulation box's X-Y area (*i.e.*, the average bilayer's projected area).[29] The mismatch area between the two domains, $\Delta A = (1 - \alpha)A_o$, quantifies the overall extent to which the upper and lower leaflets are out of kilter. In this expression A_o is the L_o average domain area, and _ is the overlap fraction between domains as defined and computed in ref. 3. Figs. S3 & S4 (ESI) show the excess and mismatch areas as a function of time; $t = 0$ marks the pore-creation point. Clearly, both quantities reach maximum values when the pores lie in the more rigid L_o phase; as they move and enter the fluid phase, stress is released, flattening the membrane with both parameters assuming values close to non-porated-bilayer observations.

Localization of pores in L_d domains is demonstrated in Fig. 3, depicting histograms of the closest pore-to-domain distance, d, computed after 1 μs, *i.e.*, after $d(t)$ exhibits stationary fluctuations around a mean (cf. Fig. 2 – upper panel). As mentioned, different ξ_0 values correspond to distinct pore radii, R (the $\xi \rightarrow$R mapping is shown in Fig. S5, ESI). Clearly, on average, both hydrophilic and hydrophobic pores sit at the L_d-domain centre but diffuse freely along the y-direction of the simulation cell, i.e. parallel to the domain borders (see movie files provided as ESI). The d-distribution is broad, but pores never 'pin' to the borders. This demonstrates that transmembrane pores do not enter spontaneously the L_o-phase, and whenever they are created in the rigid phase, stress builds up, mobile lipids enrichen the pore border and they carry it to L_d.

View Article Online
DOI: 10.1039/C8CP00958A

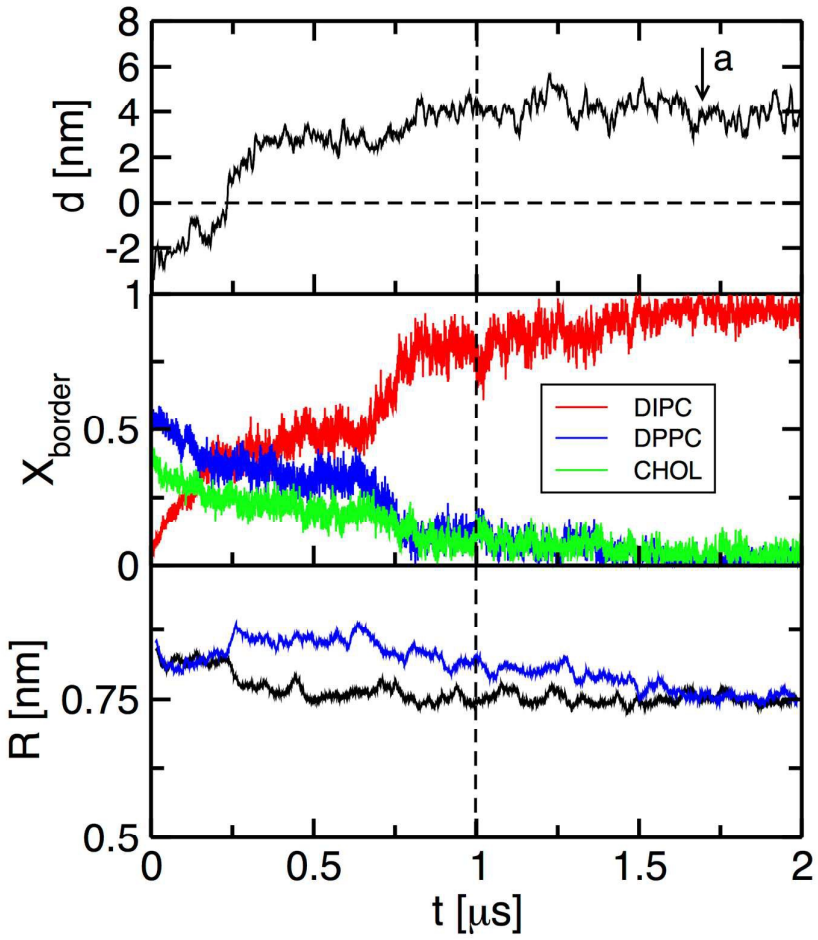

Figure 2: Upper panel: time evolution of the distance of closest approach, d, between the pore centre and the domain border. d<0 implies that the pore is in the L_o domain. The arrow-marked point on the d-curve corresponds to the configuration shown in the final panel of Fig. 1. Central panel: pore border composition ($X_{i,border} = N_i / (N_{DPPC} + N_{DIPC} + N_{Chol})$) showing DIPC recruitment (and DPPC+CHOL depletion). Notice that the border composition plateaus after ~1 μs upon pore stabilisation at the L_d-domain centre. Bottom panel: time evolution of the pore radius (R). In the three panels the data correspond to one of the two independent trajectories for the largest pore (ξ_0 =0.8, R~1nm). All the simulations started from a configuration where the pore was created at the centre of the L_o-domain. Fig. S2 shows the pore radius time series for all the cases investigated.

View Article Online
DOI: 10.1039/C8CP00958A

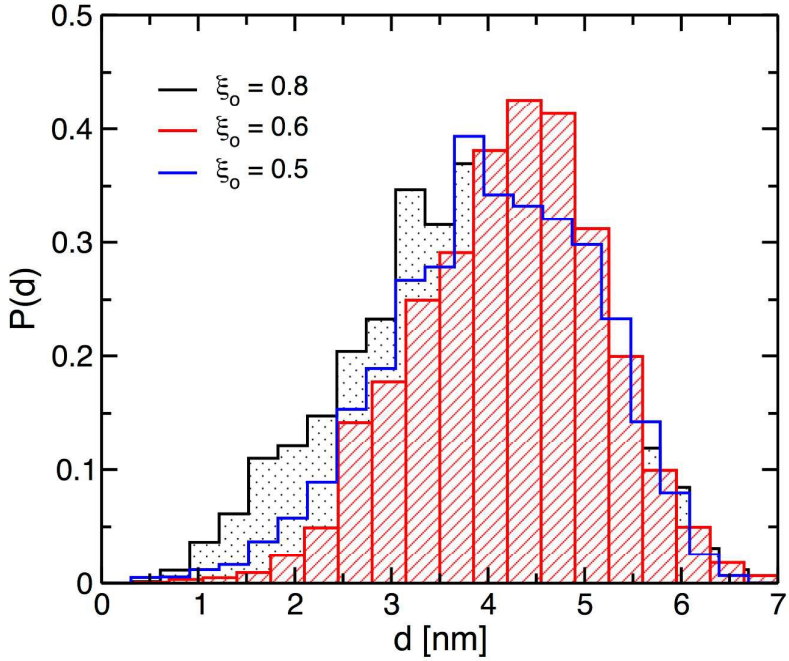

Figure 3: *Histograms of the closest pore-to-domain distance, d, computed after 1 μs, i.e., after d(t) exhibits stationary fluctuations around a mean (cf. Fig. 2 - upper). On average, both hydrophilic and hydrophobic pores sit at the L_d-domain centre but diffuse parallel to the domain borders (see movie files, ESI). The d-distribution is broad. Pores never 'pin' to the border nor enter L_o spontaneously.*

Pore-nucleation energetics was investigated via US, following the procedure described above; calculations were performed on pure L_d and L_o bilayers and a phase-segregated bilayer. In the latter case, each US window's initial configuration had the pore centred in the L_d domain to accelerate equilibration. Fig. 4 shows $\Delta G(\xi)$ and $\Delta G(R)$ in the upper and lower panels, respectively. The three $\Delta G(\xi)$ curves evince similar qualitative trends: a deep minimum at the equilibrium membrane density, $\xi \sim 0$, followed by a smooth increase and a pronounced slope change between $\xi \sim 0.35$ and 0.5, depending on system composition. Inspection of trajectories reveals that, before the inflection point, the membrane sustains a small, fluctuating, and fairly irregular hydrophobic defect. The $\Delta G(\xi)$ inflection coincides with something qualitatively different: the appearance of a thin water channel extending across the membrane. From then on, increasing ξ values lead to progressively larger hydrophilic pores that, on average, have a toroidal shape with radius R. Notice that R serves as a meaningful descriptor of the pore shape when the hydrated pore is relatively large.

View Article Online
DOI: 10.1039/C8CP00958A

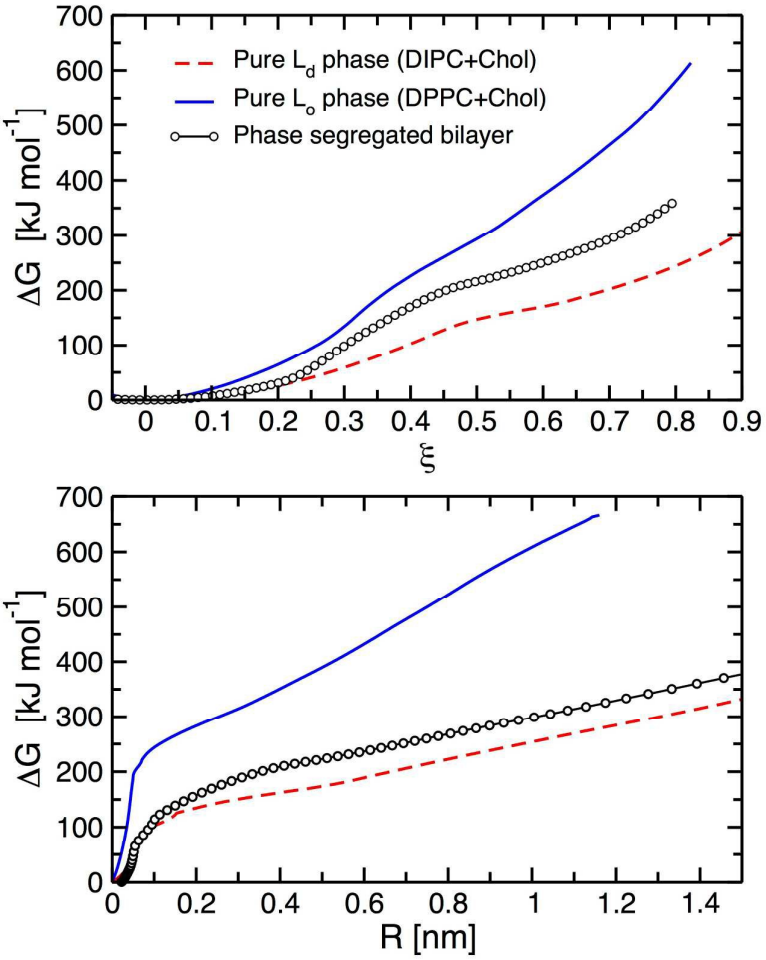

Figure 4: *Pore formation free energies ΔG(ξ) and ΔG(R) for a pure L_o bilayer (continuous blue lines), a pure L_d phase (dashed red lines), and the phase segregated membrane (black lines with circles). The functional relationship R(ξ) is shown in Fig. S5 (ESI). The inflection point in ΔG(ξ) allows to identify ΔG_n, which marks the appearance of the first hydrophilic pore. Straight-line fittings to the linear regions of ΔG(R) allow to extract the membrane line tension γ_L. Notice that pores of any size are created more easily in L_d. For the phase-segregated system, creating a pore in the L_d domain is slightly costlier than in the bulk of a pure L_d phase, suggesting the domain borders proximity renders the pore more unstable.*

The standard phenomenological pore-nucleation model states that the pore's free energy can be written as[9,12-15]

$$\Delta G(R) = \Delta G_n + 2\gamma_L \pi R - \pi \gamma_s R^2$$

View Article Online
DOI: 10.1039/C8CP00958A

where ΔG_n is a constant, R denotes pore radius, γ_L is the bilayer/water-border line tension, and γ_S is the lateral tension imposed on the membrane. ΔG_n is identified as the cost of creating a first hydrated transmembrane defect. Fig. 4's $\Delta G(R)$ curves show deep quadratic minima followed by a linear function, as our simulations were performed under the standard condition of zero-lateral-tension (γ_s=0). The overall shape of these curves coincides with the free-energy profiles reported by Tolpekina et al.[12] and by Wohlert et al.[14] for single component L_d-membranes. Such similarity is expected, considering that the pore nucleation mechanisms observed in our systems go through the two standard stages as the pore size increases, i.e. small pores (or defects) are hydrophobic, large pores are hydrophilic.[12,14] In the latter case, the lipids that make up the border of the pore reorient themselves exposing the hydrophilic head to the water bridge that crosses the membrane.

For the three systems under consideration straight line fittings to the $\Delta G(R)$ curves (see Fig. S7 for details) deliver: ΔG_n^{Lo}= 192 kJ/mol, ΔG_n^{Ld} =101 kJ/mol, and ΔG_n^{PS}=146 kJ/mol for the phase segregated system (PS); and line tensions of γ_L^{Lo}=108.6 pN, γ_L^{Ld}= 40.1 pN, and γ_L^{PS}= 40.4 pN. Notice that in all cases the value of ΔG_n obtained by fitting equation 1 to $\Delta G(R)$ is ~19% lower than the value of $\Delta G(\xi)$ when the first hydrophilic pore is formed, *i.e.* the value of $\Delta G(\xi)$ at the inflection point of the curves in the upper panel of Fig. 4: ΔG_{inf}^{Lo}= 230 kJ/mol, ΔG_{inf}^{Ld} = 120 kJ/mol and ΔG_{inf}^{PS} = 175 kJ/mol. The difference between ΔG_n and ΔG_{inf} is expected, however, and can be attributed to the limitations of Classical Nucleation Theory (equation 1) to describe the formation of very small pores (R < 0.3nm). All considered, the values of ΔG_{inf}, ΔG_n, and γ_L show that pores of any size are more easily created in the bulk of the L_d phase. Whenever they are created in L_o there is a large thermodynamic driving force, of, *e.g.* ~250 & 350 kJ/mol for respective radii of ~0.5 & 1 nm, pushing them to L_d (see Fig. S6, ESI). Furthermore, Fig. 4 shows that creating a pore in the L_d domain of a phase-segregated bilayer is slightly costlier than in the bulk of L_d. This result suggests that the proximity of the domain borders renders the pore more unstable, probably due to repulsive elastic interactions between the pore edge and the $L_d - L_o$ interphase, although membrane bending could also be partially responsible for this effect. Indeed, pore-induced curvature is not observed, for any pore size, when pores are created in the bulk of L_o or L_d phases, suggesting that the transient curvatures observed in Fig. 1 are related to the distribution of tensions in the porated phase-segregated system.

View Article Online
DOI: 10.1039/C8CP00958A

In an instructive paper,[19] Reigada has discussed the electroporation kinetics of a phase-segregated membrane under large transmembrane electric fields. Atomistic MD simulations show that disordered membranes electroporate more quickly than ordered membranes; that electroporation occurs preferentially in L_d domains, with rupture times shorter for smaller domains; and that electropores show no affinity for domain boundaries. Although the free-energy profiles of Fig. 4 were computed under no electric field, our results provide thermodynamic support and a concurrent interpretation of the kinetic data reported in Ref. 19. It remains to be seen whether the increased pore-nucleation susceptibility of the nanometric L_d -domains investigated in those simulations, is a direct consequence of the large transmembrane field, a finite size effect, or a combination of both. In the meantime, our results indicate that pore nucleation in a relatively narrow but semi-infinite L_d-slab is costlier (45 kJ/mol for R > 0.5nm) than in the bulk of L_d.

In closing, we studied transmembrane-pore formation via coarse-grained Molecular Dynamics on a segregated lipid bilayer formed by DIPC, DPPC and cholesterol, finding that pores created in L_o domains always migrate spontaneously to L_d, by recruiting mobile, unsaturated DIPC lipids to the pore's rim to transport the pore to the fluid phase. Once in L_d, pores migrate towards its centre, never returning to L_o or binding to the domain borders. Free-energy calculations quantify the actual thermodynamic driving force that pushes and confines the pores, of nanometric dimensions, to L_d domains. On one side, our results explain why electro-pores are experimentally observed in L_d; on the other, the DIPC 'cloaking' mechanism revealed by the simulations points to a line-tension moderation mechanism (*i.e.*, border recruitment of unsaturated lipids) that offers the intriguing possibility to aid nanoparticle- or macromolecule- diffusion in lipid-bilayer systems by amassing a mobile-lipid skin.

Supporting Information

Local composition across the phase-segregated membrane. Movie files. Pore radii as a function of time. Time evolution of membrane excess area. Time evolution of mismatch area between domains' upper and lower leaflets. Functional relationship between the order parameter ξ and pore radius R. Difference in free-energy cost for creating pores in the bulk of L_o or L_d phases, *i.e.*, $\Delta G_{Ld}(R) - \Delta G_{Lo}(R)$. Least-square fittings of $\Delta G(R)$ to the Classical Nucleation Theory expression.

View Article Online
DOI: 10.1039/C8CP00958A

Acknowledgements

All the authors thank funding from the EC-H2020-MSC-RISE-2014 programme, through project 643998 ENACT. M.G.D.P acknowledges financial support from CONICET, SECTyP, UNCUYO, FONCyT (PICT-2012-2759), and SNCAD-MinCyT for computer-time allocation in the clusters Mendieta (CCAD-UNC) and Toko (UNCUYO).

View Article Online
DOI: 10.1039/C8CP00958A

References

1. T. Heimburg, Thermal Biophysics of Membranes, **2007**, WILEY-VCH Verlag GmbH & Co. KGaA.
2. W.F.D. Bennett, D.P. Tieleman, Computer simulations of lipid membrane domains, *Biochim. Biophys. Acta*, **2013**, *1828*, 1765–1776.
3. H. Jelger Risselada, S.J. Marrink, The molecular face of lipid rafts in model membranes, *Proc. Nat. Acad. Sci.*, **2008**, *105*, 17367–17372.
4. D. Hakobyan, A. Heuer, Key Molecular Requirements for Raft Formation in Lipid/Cholesterol Membranes, *PLoS ONE*, **2014**, *9*, e87369.
5. D. Papahadjopoulos, K. Jacobson, S. Nir, and T. Isac. Phase transitions in phospholipid vesicles. fluorescence polarization and permeability measurements concerning the effect of temperature and cholesterol. *Biochim. Biophys. Acta*, **1973**,311:330–340.
6. V.F. Antonov, V.V. Petrov, A.A. Molnar, D.A. Predvoditelev, A.S. Ivanov, The appearance of single-ion channels in unmodified lipid bilayer membranes at the phase transition temperature. *Nature* **1980**, *283*, 585-586.
7. L. Cruzeiro-Hansson and O. G. Mouritsen. Passive ion permeability of lipid membranes modelled via lipid-domain interfacial area. *Biochim. Biophys. Acta*, **1988**, 944:63–72.
8. J.T. Sengel, M.I. Wallace, Imaging the dynamics of individual electropores, *Proc. Nat. Acad. Sci.*, **2016**, *113*, 5281–5286.
9. G. Fuertes, D. Giménez, S. Esteban-Martín, O. L. Sánchez-Muñoz, J. Salgado, A lipocentric view of peptide-induced pores, *Eur. Biophys. J.*, **2011**, 40:399–415.
10. V. Talanquer, D.W. Oxtoby, Nucleation of pores in amphiphile bilayers, *J. Chem. Phys.*, **2003**, *118*, 872-877.
11. S. J. Marrink and D.P. Tieleman, Perspective on the Martini Model, *Chem. Soc. Rev.* **2013**, *42*, 6801.
12. T.V. Tolpekina, W.K. den Otter, W.J. Briels, Nucleation free energy of pore formation in an amphiphilic bilayer studied by molecular dynamics simulations, *J. Chem. Phys.*, **2004**, *121*, 12060-12066.
13. Z.-J. Wang and D. Frenkel, Pore nucleation in mechanically stretched bilayer membranes, *J. Chem. Phys.* **2005**, *123*, 154701.
14. J. Wohlert, W. K. den Otter, O. Edholm, and W. J. Briels, Free energy of a trans-membrane pore calculated from atomistic molecular dynamics simulations, *J. Chem. Phys.* **2006**, *124*, 154905.

View Article Online
DOI: 10.1039/C8CP00958A

15. W.K. den Otter, Free energies of stable and metastable pores in lipid membranes under tension, *J. Chem. Phys.* **2009**, *131*, 205101.

16. R. Notman, J. Anwar, W.J. Briels, M.G. Noro, W.K. den Otter, Simulations of skin barrier function: free energies of hydrophobic and hydrophilic transmembrane pores in ceramide bilayers, *Biophys J.*, **2008**, *95*, 4763-71.

17. L. Delemotte, M. Tarek, Molecular Dynamics Simulations of Lipid Membrane Electroporation, *J. Membrane Biol.*, **2012**, *245*, 531–543.

18. F. Dehez, L. Delemotte, P. Kramar, D. Miklavčič, M. Tarek, Evidence of Conducting Hydrophobic Nanopores Across Membranes in Response to an Electric Field, *J. Phys. Chem. C* **2014**, *118*, 6752−6757.

19. R. Reigada, Electroporation of heterogeneous lipid membranes, *Biochim. Biophys. Acta*, **2014**, *1838*, 814-821.

20. W.F.D. Bennett, D.P. Tieleman The Importance of Membrane Defects - Lessons from Simulations, *Acc. Chem. Res.*, **2014**, *47*, 2244–2251.

21. S.J. Marrink, A.H. de Vries, D.P. Tieleman, Lipids on the move: Simulations of membrane pores, domains, stalks and curves, *Biochim. Biophys. Acta*, **2009**, *1788*, 149–168.

22. I. Vorobyov, T.E. Olson, J.H. Kim, R.E. Koeppe II, O.S. Andersen T.W. Allen, Ion-Induced Defect Permeation of Lipid Membranes, *Biophys J.*, **2014**, *106*, 586-597.

23. H.J.C.Berendsen, D.van der Spoel, R.van Drunen, GROMACS: A message-passing parallel molecular dynamics implementation, *Comput. Phys. Commun.*, **1995**, *91*, 43-56.

24. S. Pronk, R. Schulz, P. Larsson, P. Bjelkmar, R. Apostolov, M. R. Shirts, J. C. Smith, P. M. Kasson, D. van der Spoel, B. Hess and E. Lindahl, *Bioinformatics*, **2013**, 29, 845.

25. T. Darden, D. York and L. Pedersen, *The Journal of Chemical Physics*, **1993**, 98, 10089–10092.

26. T. Darden, L. Perera, L. Li, L. Pedersen, L (1999). New tricks for modelers from the crystallography toolkit: the particle mesh Ewald algorithm and its use in nucleic acid simulations, *Structure*, **1999**, *7*, R55–R60.

27. M. Bonomi, D. Branduardi, G. Bussi, C. Camilloni, D. Provasi, P. Raiteri, D. Donadio, F. Marinelli, F. Pietrucci, R.A. Broglia, M. Parrinello, PLUMED: A portable plugin for free-energy calculations with molecular dynamics, *Computer Physics Communications*, **2009**, *180*, 1961-1972.

28. S. Kumar, J.M. Rosenberg, D. Bouzida, R.H. Swendsen, P.A. Kollman, The weighted histogram analysis method for free-energy calculations on biomolecules. I. The method, *J. Comput. Chem.* **1992**, *13*, 1011–1021.

29. V. Gapsys, B. L. de Groot, R. Briones, Computational analysis of local membrane properties, J *Comput. Aided Mol. Des*. **2013** 27:845–858.

30. Tribello, G. A.; Bonomi, M.; Branduardi, D.; Camilloni, C.; Bussi, G. PLUMED 2: New feathers for an old bird. *Computer Physics Communications,* **2014**, 185, 604–613.